CHALMERS
UNIVERSITY OF TECHNOLOGY

A high-gain gap waveguide-based 16 × 16 slot antenna array with low sidelobe level for mmwave applications

scientific reports

Check for updates

OPEN

A high-gain gap waveguide-based 16 × 16 slot antenna array with low sidelobe level for mmwave applications

Davood Zarifi[1,2]✉, Ali Sabbaghi Saber[1] & Ashraf Uz Zaman[3]

This study presents the design of a high-gain 16 × 16-slot antenna array with a low sidelobe level (SLL) using a tapered ridge gap waveguide feeding network for Ka-band applications. The proposed antenna element includes four cavity-backed slot antennas. A tapered feeding network is designed and utilized for unequal feeding of the radiating elements. Ridge gap waveguide technology is used to reduce the feeding network loss and achieve a low-loss array antenna. The feed layer of the proposed antenna is coupled to a standard rectangular waveguide (WR-28) using a proper transition. The measured results show an impedance bandwidth of more than 17% over the frequency range of 27.5–32.6 GHz covering one of the standard vehicle-to-satellite band (29.4–31.0 GHz) and 5G mmWave N261 band (27.5–28.35 GHz), a maximum gain of 28.9 dBi, and SLL lower than − 20 dB. Thanks to its high performance and desirable features, the proposed antenna shows potential for use in vehicular radar systems and high data rate mmWave communications.

With the development of Internet of vehicles (IoV), reliable high-speed communication systems have drawn great attention[1]. The high-performance antennas exhibiting high gain, low SLL and acceptable bandwidth are one of the critical and key components to improve performance of wireless transceiver frontends. The application of a high-performance antenna array in IoV sensing and communication is illustrated in Fig. 1. An antenna array mounted in a vehicle can be employed to communicate with the satellite and also for sensing surrounding objects. Using a high-performance antenna array results in increasing signal-to-noise-ratio, data rate and channel capacity, in the mmWave frequency bands.

In recent years, mmWave antenna arrays with high gain and low sidelobe levels (SLL) have attracted a huge deal of use in various applications for minimizing interferences from other wireless systems. Both reflector and array antennas can be created with lower SLL through an array rather than a reflector. Amplitude tapering is the most common method to reduce the SLL of a uniform array. Lower SLL levels in far-field patterns can be obtained by applying an appropriate feed network to weight the power applied to each element. However, due to the mutual coupling of surface waves and radiating elements, it is challenging to realize the arrays with low SLL for planar arrays. Moreover, when a lower SLL is required in a wide- bandwidth, it is essential to accept a lower gain as a compromise.

According to the literature, various microwave and mmWave applications can be performed using low SLL antennas like parabolic reflector antennas[2], printed antennas[3–7], and waveguide-based slot array antennas[8–14]. In[8], a circular aperture array antenna with tapering the amplitude in the distribution network is utilized to suppress SLL. Nevertheless, the array antenna bandwidth is constrained exceptionally owing to the series-fed configuration. In[9], a Ku-band slot array antenna was proposed to feed a hollow waveguide via the Taylor distribution. In[10], a low SLL 32 × 64-element slot array antenna was proposed based on a nonuniform corporate-feed-network. Its main drawback is complexity, which leads to the need for a precision manufacturing process. Anyway, an array antenna has a costly and complicated manufacturing procedure. At mmWave frequencies, dielectric substrate-based large high-gain low SLL antenna arrays suffer from dielectric loss and undesired surface radiations. Although waveguide-based slot antenna arrays have low-loss structures, they have large sizes and need high precision and high-cost fabrication processes to overcome electric connection challenges.

[1]School of Electrical and Computer Engineering, University of Kashan, Kashan, Iran. [2]Department of Microwave and Antenna Engineering, Faculty of Electronics, Telecommunications, and Informatics, Gdańsk University of Technology, Gdańsk 80-233, Poland. [3]Department of Electrical Engineering, Chalmers University of Technology, Gothenburg, Sweden. ✉email: davood.zarifi@pg.edu.pl

Fig. 1. Application of a high-performance antenna in vehicular sensing and communication.

Recently, a large development took place in the field of slot array using gap waveguide technology to design, implement, and fabricate high performance mmWave antennas[14–19]. Gap waveguide technology has the advantages of a simple manufacturing process, low loss, and easy integration. Recently, several gap waveguide-based low SLL antenna arrays have been proposed in the literature for different mmWave applications and compact RF front ends can be built based on gap waveguide technology[20–29]. In these designs, gap waveguide technology is a novel technology to solve manufacturing problems. In[20], the slot array antennas were rotated to obtain qualified radiation with low SLL. Nevertheless, this technique cannot reduce the SLL of the radiation pattern at every azimuth angle. In[23], an inadequate power divider oriented by an inverted microstrip gap waveguide was proposed to design a low SLL 16 × 16 antenna array. The SLL of the array antenna is less than − 23 dB on both the H- and E- planes with 18.5% impedance bandwidth at 40 GHz. However, the antenna efficiency is reduced to 50% because of using a dielectric substrate. In[24], a 16 × 16-element antenna array was proposed with a gain > 28 dBi over the operating frequency band of 27.4–28.6 GHz. In that design, a multilayer low-loss gap waveguide-based tapered feeding network was applied to reduce SLL to −19dB. In[26], a low SLL antenna array has been proposed based on gap and hollow waveguides with impedance bandwidth of 12.6% and efficiency of 35%. In[27], a ridge gap waveguide-based H-plane horn antenna has been proposed with 25% fractional bandwidth, peak gain of 10.7 dBi and SLL < −20dB[27]. Although that work exhibits acceptable bandwidth and SLL, it has certain limitations such as low gain and wide beam in H-plane. More recently, a low SLL slot array antenna has been proposed with SLL < −21dB, minimum gain of 25.5 dB, 10.98% fractional bandwidth and efficiency of 82%[29].

Generally, the mentioned slot array antennas are relatively narrow-band and complicated owing to the multilayer structures with a high-cost and complex fabricating procedure. Such unwanted features are drawbacks preventing their usage in for utilizing in IoV and 5G mmWave communications. With the variety of satellite frequency bands that can be used, designations have been developed so that they can be referred to easily. For instance, in the vehicle-to-satellite links, the frequency range from 27.5 GHz to 31 GHz bands is utilized for high-resolution and close-range targeting. In[30–34], wideband antennas for the IoV have been proposed. Despite having excellent characteristics, they cannot satisfy the low SLL requirements.

To the best knowledge of the authors, the capability of gap waveguide technology in the design and implementation of wideband low antenna arrays with high-gain, wide bandwidth and low SLL that can meet the desired requirement of the IoV has not been demonstrated in the literature. In the present research, a ridge gap waveguide is applied to design a.

low SLL antenna array. It aimed to design a high-gain cavity-backed 16 × 16-element slot array.

antenna with lower SLL features over 17% relative bandwidth covering one of the standard vehicle-to-satellite band (29.4–31.0 GHz) and 5G mmWave N261 band (27.5–28.35 GHz). As the main loss in an array antenna is due to its feeding network, the feeding losses are eliminated using a ridge gap waveguide, thereby achieving a high-performance antenna array. In this design, a low-loss ridge gap waveguide-based feeding network with Taylor distribution is employed to reduce SLL to −20 dB.

Gap waveguide concept

The gap waveguide concept leverages boundary conditions to direct electromagnetic waves within a parallel-plate waveguide. This structure uses perfect electric conductors (PEC) and perfect magnetic conductors (PMC)

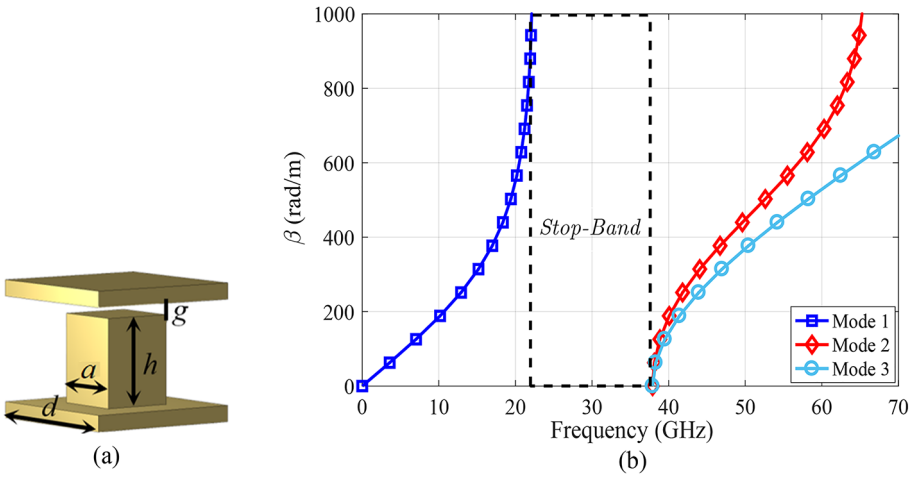

Fig. 2. (**a**) Configuration of the unitcell of periodic pins structure and (**b**) its dispersion diagram.

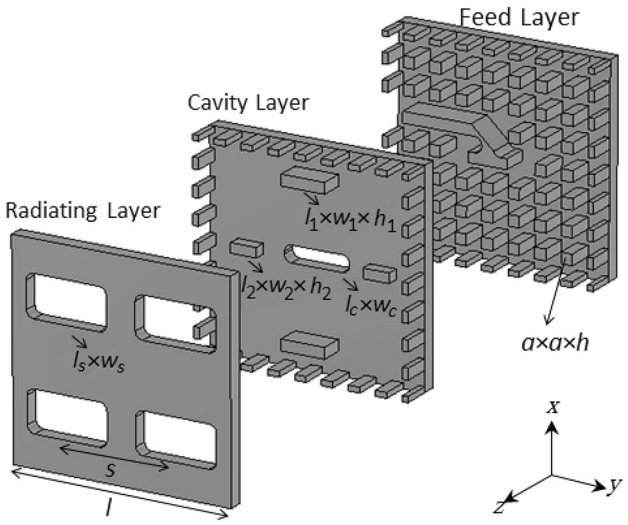

Fig. 3. Perspective view of Exploded 2 × 2-element subarray.

to form the waveguide. When the plates are spaced less than λ/4 apart, electromagnetic waves cannot propagate. The PMC surface is created using periodic metallic pins on a metal plate. By removing some rows of these pins, a waveguide mode can be established. The groove gap waveguide, similar to a rectangular waveguide, supports TE and TM modes based on its cross-sectional dimensions. In ridge, inverted-microstrip, and microstrip-ridge gap waveguides, a quasi-TEM mode can propagate. This technology eliminates the need for electrical contact between different parts of a microwave device, making it ideal for high-performance mmWave antennas and components.

The initial step in designing a gap waveguide involves selecting the dimensions of the periodic pins, as depicted in Fig. 2(a), to achieve the desired bandgap. The chosen pin dimensions are $0.8 \times 0.8 \times 2$ mm^3, with an air gap of 0.1 mm, to create a stop-band ranging from 25 to 35 GHz. The dispersion diagram for this periodic pin structure is simulated using the Eigen-mode solver in CST Microwave Studio and is shown in Fig. 2(b).

Antenna configuration

2 × 2-element subarray

Figure 3 shows the 2 × 2-element subarray structure. There are three layers in the sub-array. The feed layer is the lower layer in terms of ridge gap waveguide. A cavity includes the middle layer, which is fed by the feed layer via a rectangular coupling slot. The top layer contains the radiating slots. Four radiating slots should be equally excited by the cavity in phase and amplitude in the whole bandwidth. The cavity wall pins' positions are important as they influence the cavity resonant mode. The cavity resonant mode is controlled by the positions of the wall pins and the tuning pins' height and position.

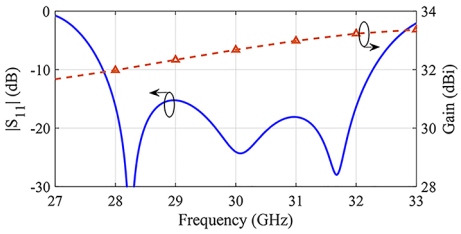

Fig. 4. |S11| and gain of 16×16-element slot array antenna.

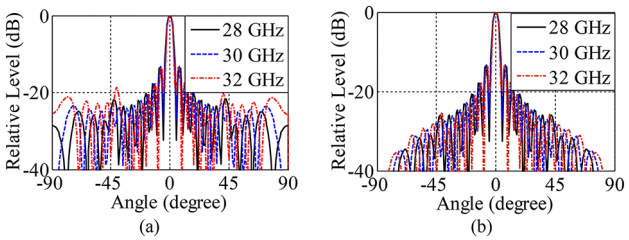

Fig. 5. Normalized radiation patterns of uniformly excited 16×16-element slot array antenna at different frequencies. (**a**) E-plane. (**b**) H-plane.

The sub-array possesses the transverse dimensions of 15 mm × 15 mm and the center-to-center spacing between the radiating slots is 7.5 mm. In the feed layer, the ridge width is 0.8 mm and at the end of the ridge, a T-shaped section is inserted to improve matching between ridge and cavity layer. The design parameters of the proposed structure are optimized via an optimization algorithm in the CST solver to achieve desired input impedance matching and high gain around 30 GHz. The optimized values of the design parameters (in mm) are $l_c = 4.57$, $w_c = 1.18$, $l_1 = 3.05$, $w_1 = 0.78$, $h_1 = 1.67$, $l_2 = 1.78$, $w_2 = 0.70$, $h_2 = 0.88$, $l_s = 5.48$, $w_s = 2.89$, and $s = 7.50$.

According to Fig. 4, the subarray simulated reflection coefficient exhibits the impedance bandwidth of 27.8–32.3 GHz for $|S_{11}| < -10$ dB. The radiation patterns of a uniformly excited 16×16-element array in E- and H-planes are determined at a frequency of 30 GHz via periodic boundary conditions in CST (Fig. 5). It is of note that the simulated peak gain is 33.2 dBi and the SLL is −13 dB in both H- and E- planes.

Feeding network

It is essential to design a full-corporate feeding network for implementing a planar array. Ridge and groove gap waveguide- based large power dividers equal power distribution have been used in previous designs[14–17]. Here, the feeding network requires unequal power distribution to decrease the SLL of the radiation pattern. As shown in Fig. 6, the proposed unequal feeding network includes several T-junction power dividers and a transition from ridge gap waveguide to standard WR-28 rectangular waveguide in the back of the feed layer.

Taylor synthesis is employed to achieve a non-uniform power distribution network to obtain the required power ratios[35]. To obtain the Taylor distribution, the amplitude for the excitation at each slot is expressed as follows:

$$I_n(r_n) = 1 + 2\sum_{m=1}^{\bar{N}-1} \bar{S}(m)\cos\left[\frac{2\pi m}{N}\left(n - \frac{N+1}{2}\right)\right] \tag{1}$$

$$\bar{S}(m) = \begin{cases} \dfrac{\left[(\bar{N}-1)!\right]^2}{(\bar{N}-1+m)!(\bar{N}-1-m)!}\displaystyle\prod_{n=1}^{\bar{N}-1}\left[1 - \frac{m^2}{\sigma^2\left(A^2 + (n-0.5)^2\right)}\right], & m \leqslant \bar{N}-1 \\ 0, & m \geqslant \bar{N} \end{cases} \tag{2}$$

$$A = \frac{1}{\pi}\cosh^{-1}(SLL_{\max}) \tag{3}$$

where r_n is the n-th slot' location in the N-element array, $\bar{N}$ is a constant design parameter and σ is the scaling factor given by

$$\sigma = \frac{\bar{N}}{\sqrt{A^2 + (\bar{N}-0.5)^2}}. \tag{4}$$

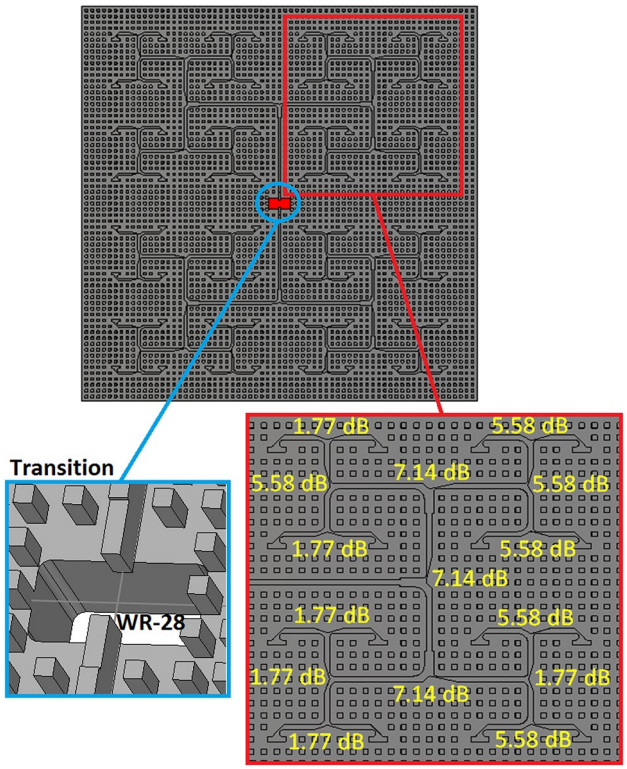

Fig. 6. Configuration of unequal feeding network including of T-junction power dividers and a transition from ridge gap waveguide to WR-28.

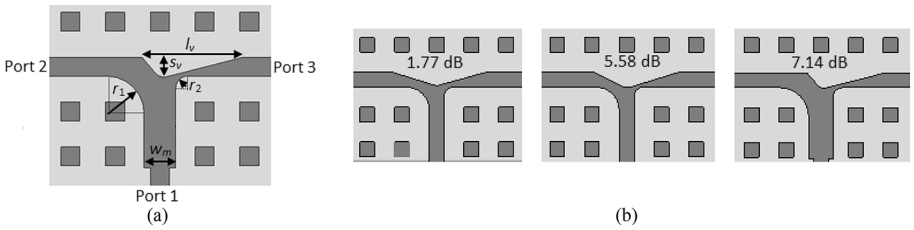

Fig. 7. (**a**) General geometry of unequal T-junction power divider. (**b**) Optimized T-junction power dividers with different power ratio. The values of geometrical parameters of three T-junction power dividers are in mm: lv = (5.14, 4.49, 4.28), sv = (0.69, 0.81, 0.83), wm = (0.8, 0.80, 1.00), r1 = (1.14, 1.37, 1.59) and r2 = (0.50, 0.50, 0.50).

Based on the Taylor distribution concept assuming $\bar{N}=4$, the considered power ratios 1.77 dB, 5.58 dB and 7.14 dB are sufficient to guarantee the SLL less than − 25 dB at 30 GHz.

Due to the symmetry of the entire feed network in both the x and y directions, Fig. 6 displays only the amplitude distribution for one quarter of the network. An effective technique to design unequal-power and equal-phase split is to change the width of connected branches to an asymmetric V-shaped section to adjust the power ratio. Figure 7 presents the configuration of the proposed 1.77 dB, 5.58 dB, and 7.14 dB T-junction power dividers. In this method, the left and right corners of the T-junction are rounded with different radius such that the desired power ratio can be achieved and the structure can be fabricated without challenges using conventional CNC milling.

Notably, the structure parameters should be optimized to achieve the desired power ratio between the output ports of the T-junction and matching at the input port. Figures 8 and 9 present the simulation results of S-parameters and electric field distribution for proposed T-junctions with different power ratios. Observe that the proposed structures exhibit excellent matching and power distribution ratios. As can be seen, the phase differences between output ports in three cases are less than ±5° over the frequency bandwidth from 27 to 33 GHz.

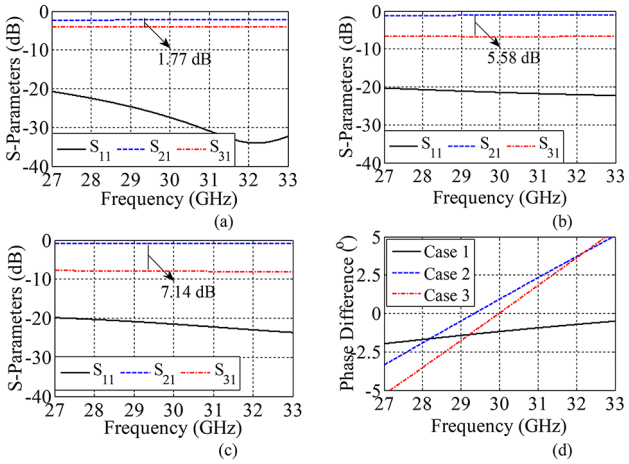

Fig. 8. Simulation results of unequal T-junction power dividers. (**a**)-(**c**) Amplitude of S-parameters. (**d**) Phased difference of output ports.

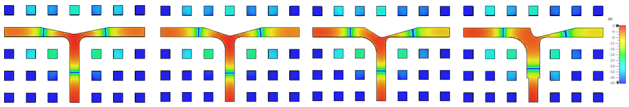

Fig. 9. Electric field distributions of T-junction power dividers at 30 GHz.

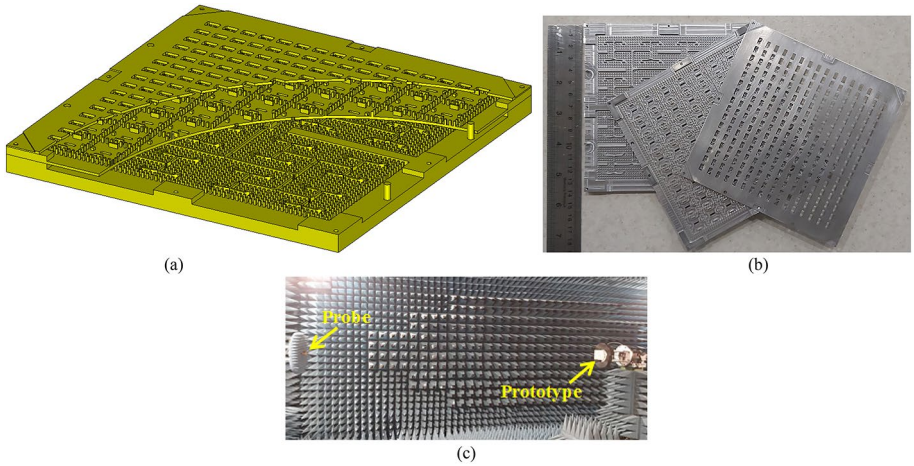

Fig. 10. (**a**) The configuration of complete 16×16-element slot array antenna. (**b**) Photograph of the fabricated prototype. (**c**) Photograph of the antenna under test in far-field test system.

Full array configuration

The complete 16×16-element slot array antenna is obtained by combining the proposed subarray and the power divider. Figure 10(a) shows the configuration of the non-uniformly excited planar array antenna. In this configuration, four ridge gap waveguide-based 1-to-16 unequal power dividers are deployed to excite 64 cavities, each exciting four radiating slots. The size of the proposed planar antenna array including the screws and side support is 115 mm × 115 mm × 10 mm. The length and height of steps at the end of ridges in the transition region are 2.36 mm and 0.23 mm, respectively. The simulated reflection coefficient, radiation pattern, and gain of the whole antenna accompanied by the measured results are provided in the following section.

Fabrication and measurement

Prototype fabrication and measurement

The design is validated by fabricating a test sample of the proposed antenna with Aluminum using a SPINNER computerized numerical control machine with position accuracy better than 12 μm and surface smoothness of

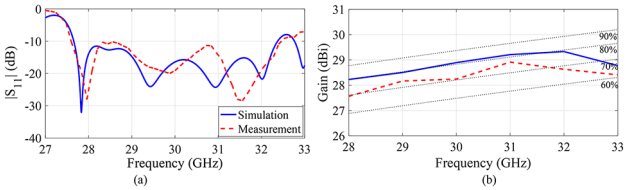

Fig. 11. Simulated and measured |S11| and gain of 16×16-element slot array antenna.

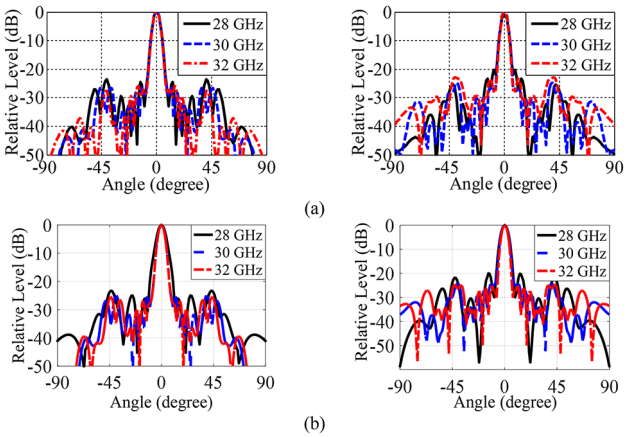

Fig. 12. Normalized radiation patterns of 16×16-element slot array antenna at different frequencies in H- and E-planes. (**a**) Simulation results. (**b**) Measurement results.

up to 0.8 μm. Figure 10(b) presents the disassembled prototype, the structure details of its different layers, and the test environment. Eight screws around the structure are employed to stack the layers up. In addition, four guiding pins are applied to ensure the alignment of the structure's three layers.

To measure the radiation performance of the fabricated antenna array, a far-field antenna test system is adopted in an anechoic chamber in the Advanced Antenna Lab at Chalmers University of Technology, as illustrated in Fig. 10(c). Figure 11(a) displays the measurement and simulation results for the antenna array's input reflection coefficient. Based on the measurements, the input reflection coefficient is below −10 dB over the frequency band from 27.5 to 32.6 GHz. The simulated and measured frequency characteristics of the realized boresight gain are depicted in Fig. 11(b). The dotted lines indicate the maximum available directivity of the antenna at efficiencies of 90%, 80%, and 70% and 60%. The measured peak gain is 28.9 dBi over the desired frequency bandwidth and the antenna efficiency is better than 65% from 27.5 to 32.6 GHz. The measurement involves some gain variations owing to the measurement tolerance and non-stable amplitude tapering distribution and phase with frequencies. Figure 12 illustrates the measured and simulated normalized radiation patterns at 28, 30, and 32 GHz on both E- and H- planes. As can be seen, the measured SLL of the radiation pattern in 30 GHz is −25.7 dB. Meanwhile, it is still less than −20 dB in edge frequencies, which is a reasonable value.

Discussion

In Table 1, the performances of several reported antenna arrays are compared with the present work. The presented antenna array is a three-layer structure with acceptable IBW bandwidth (17%), SLL (−20dB), and gain (28.9 dBi) compared with similar arrays. The main advantage of the proposed antenna compared to hollow waveguide-based antennas[9–13]is to overcome the manufacturing challenges in mmWave frequencies because of using gap waveguide technology. The design and fabrication of the array antennas presented in[21–23] was based on the printed gap waveguide technology, which resulted in efficiencies of less than 50%. The dielectric and ohmic losses of the present work are relatively lower than those of PCB- based antennas due to using the ridge gap waveguide-based feeding network resulting in 65% antenna efficiency. The proposed antenna array could be an appropriate candidate for mmWave and IoV applications requiring low SLL in the standard vehicle-to-satellite band (29.4–31.0 GHz) and 5G mmWave N261 band (27.5–28.35 GHz).

Conclusion

A high-gain low SLL slot antenna array is presented based on gap waveguide technology. The feeding network is designed as a low-loss tapered unequal power divider to achieve a radiation pattern with low SLL. The ultimate structure is an array with 16×16-element fed by a standard WR-28 waveguide. The measurement results reveal an impedance bandwidth of 17% with a center frequency of 30.05 GHz, peak gain of 28.9 GHz, and

Ref	Technology	f_0 (GHz)	Bandwidth (%)	Size of Array	Gain (dBi)	SLL (dB)	Efficiency (%)
[5] 2022	SIW	10	7.15	6×16	21.92	-29.1	NA
[7] 2023	SIW	94	3.7	16×16	25.5	-16.3	61.2
[9] 2015	Hollow Waveguide	15.2	13.8	16×16	30.2	-23	60
[10] 2018	Hollow Waveguide	74	10.8	16×16	32.8	-20	70
[12] 2022	Hollow Waveguide	78.5	19.2	8×8	25.5	-21	70
[13] 2023	Hollow Waveguide	15.2	8.4	16×16	25.4	-22	60
[21] 2019	Gap Waveguide	37.5	18.7	8×8	24.2	-18	41.7
[22] 2020	Gap Waveguide	34	33	4×4	17.2	-14	30
[23] 2021	Gap Waveguide	40	18.5	16×16	29.9	-23	50
[24] 2022	Gap Waveguide	28	4.3	16×16	28	-18.5	50
[25] 2023	Gap Waveguide	93	3	2×24	23.5	-26	85
[26] 2023	Gap Waveguide	40	12.6	16×16	29	-22.5	35
[28] 2024	Gap Waveguide	34.5	2.9	1×8	17.3	-19.4	60
[29] 2024	Gap Waveguide	30	10.98	8×8	25.5	-21	82
This Work	Gap Waveguide	30.05	17	16×16	28.9	-20	65

Table 1. Comparison with some other low SLL array antenna.

SLL lower than − 20 dB. The proposed configuration can have significant commercial applications in mmWave communication systems and radars.

Data availability

All data generated or analysed during this study are included in this published article.

Received: 13 August 2024; Accepted: 12 December 2024
Published online: 28 December 2024

References

1. Chen, C., Wu, J., Lin, H., Chen, W. & Zheng, Z. A Secure and Efficient Blockchain-Based Data Trading Approach for Internet of Vehicles, *IEEE Transactions on Vehicular Technology*, vol. 68, no. 9, pp. 9110–9121, Sept. (2019).
2. Kishk, A. A. & Shafai, L. Small reflector antenna with low sidelobes. *IEEE Trans. Antenna Propag.* **51** (10), 2907–2912 (2003).
3. Park, S. J., Shin, D. H. & Park, S. O. Low Side-Lobe Substrate-Integrated-Waveguide Antenna Array Using Broadband Unequal Feeding Network for Millimeter-Wave Handset Device. *IEEE Trans. Antennas Propag.*, **64**, 3, pp. 923–932, March 2016.
4. Cheng, Y. J., Wang, J. & Liu, X. L. 94 GHz substrate integrated waveguide dual-circular-polarization shared-aperture parallel-plate longslot array antenna with low sidelobe level, *IEEE Trans. Antennas Propag.*, vol. 65, no. 11, pp. 5855–5861, Nov. (2017).
5. Trinh, T. V., Trinh-Van, S., Lee, K. Y., Yang, Y. & Hwang, K. C. Design of a low-cost low-sidelobe-level differential-fed SIW slot array antenna with zero beam squint. *Appl. Sci.* **12** (21), 10826 (Oct. 2022).
6. Tsai, C. E. et al. A 60 GHz Rhombic Patch Array Antenna with High Gain, Low Sidelobe Level, and Reduced Array Area. *IEEE Access.* **10**, 86498–86509 (2022).
7. Wu, Y. F., You, Q., Zhang, Y., Guo, Y. & Cheng, Y. J. Sidelobe Level Reduction for a W-Band SIW Slot Array Antenna by Only Reversing Offset Direction of Partial Slots, in *IEEE Transactions on Antennas and Propagation*, vol. 71, no. 10, pp. 8360–8365, Oct. (2023).
8. Kumar, P., Kedar, A. & Singh, A. K. Design and development of low-cost low sidelobe level slotted waveguide antenna array in X-band, *IEEE Trans. Antennas Propag.*, vol. 63, no. 11, pp. 4723–4731, Nov. (2015).
9. Huang, G. L., Zhou, S. G., Chio, T. H., Hui, H. T. & Yeo, T. S. A low profile and low sidelobe wideband slot antenna array Feb by an amplitude-tapering waveguide feed-network. *IEEE Trans. Antennas Propag.* **63** (1), 419–423 (Jan. 2015).
10. Qin, L. et al. Millimeter-Wave Slotted Waveguide Array with Unequal Beamwidths and Low Sidelobe Levels for Vehicle Radars and Communications, *IEEE Transactions on Vehicular Technology*, vol. 67, no. 11, pp. 10574–10582, Nov. (2018).
11. Chen, R. S. et al. Apr., Low-sidelobe cavity-backed slot antenna array with simplified feeding structure for vehicular communications, *IEEE Trans. Veh. Technol.*, vol. 70, no. 4, pp. 3652–3660, (2021).
12. Liu, P., Pedersen, G. F. & Zhang, S. Wideband Low-Sidelobe Slot Array Antenna with Compact Tapering Feeding Network for E-Band Wireless Communications. *IEEE Trans. Antennas Propag.* **70** (4), 2676–2685 (April 2022).
13. Liu, P., Pedersen, G. F., Hong, W. & Zhang, S. Dual-Polarized Wideband Low-Sidelobe Slot Array Antenna for V-Band Wireless Communications, *IEEE Transactions on Antennas and Propagation*, vol. 71, no. 8, pp. 6667–6677, Aug. (2023).
14. Zarifi, D., Farahbakhsh, A., Zaman, A. U. & Kildal, P. S. Design and Fabrication of a High-Gain 60-GHz Corrugated Slot Antenna Array with Ridge Gap Waveguide Distribution Layer. *IEEE Trans. Antennas Propag.*, **64**, 7, pp. 2905–2913, July 2016.
15. Ferrando-Rocher, M., Valero-Nogueira, A., Herranz-Herruzo, J. I. & Teniente, J. 60 GHz single-layer slot-array antenna fed by groove gap waveguide. *IEEE AntennasWireless Propag. Lett.* **18** (5), 846–850 (May 2019).
16. Ferrando-Rocher, M., Herranz-Herruzo, J. I., Valero-Nogueira, A. & Baquero-Escudero, M. Dual-band single-layer slot array antenna fed by K/Ka-band dual-mode resonators in gap waveguide technology, *IEEE Antennas Wireless Propag. Lett.*, vol. 20, no. 3, pp. 416–420, Mar. (2021).
17. Zarifi, D., Farahbakhsh, A., Zaman, A. U. & Waveguide-Based, A. G. D-Band Slot Array Antenna with Interdigital Feed Network, *IEEE Transactions on Antennas and Propagation*, vol. 71, no. 9, pp. 7124–7131, Sept. (2023).
18. Memeletzoglou, N. & Rajo-Iglesias, E. Array of stacked leaky-wave antennas in groove gap waveguide technology. *Sci. Rep.*, **11**, (2021).
19. Herrán, L. F., Brazalez, A. A. & Rajo-Iglesias, E. Ka-band planar slotted waveguide array based on groove gap waveguide technology with a glide-symmetric holey metasurface. *Sci. Rep.* **11** (1), 1–9 (2021).

20. Vosoogh, A., Kildal, P. & Vassilev, V. Wideband and high-gain corporate-fed gap waveguide slot array antenna with ETSI class II radiation pattern in *V*-band. *IEEE Trans. Antennas Propag.* **65** (4), 1823–1831 (Apr. 2017).
21. Jiang, X. et al. Jun., Ka-band 8×8 low-sidelobe slot antenna array using a 1-to-64 high-efficiency network designed by new printed RGW technology, *IEEE Antennas Wireless Propag. Lett.*, vol. 18, no. 6, pp. 1248–1252, (2019).
22. Li, T. & Chen, Z. N. Wideband sidelobe-level reduced Ka-band metasurface antenna array fed by substrate-integrated gap waveguide using characteristic mode analysis, *IEEE Trans. Antennas Propag.*, vol. 68, no. 3, pp. 1356–1365, Mar. (2020).
23. Liu, J., Yang, F., Fan, K. & Jin, C. Unequal Power Divider Based on Inverted Microstrip Gap Waveguide and Its Application for Low Sidelobe Slot Array Antenna at 39 GHz, in *IEEE Transactions on Antennas and Propagation*, vol. 69, no. 12, pp. 8415–8425, Dec. (2021).
24. Ran, J., Jin, C., Zhang, P., Wang, W. & Wu, Y. High-gain and low-loss dual-polarized antenna array with reduced sidelobe level based on gap waveguide at 28 GHz. *IEEE Antennas Wirel. Propag. Lett.* **21** (5), 1022–1026 (May 2022).
25. Yue, J., Zhou, C., Xiao, K., Ding, L. & Chai, S. W-Band Low-Sidelobe Series-Fed Slot Array Antenna Based on Groove Gap Waveguide, in *IEEE Antennas and Wireless Propagation Letters*, vol. 22, no. 4, pp. 908–912, April (2023).
26. Jiang, X. et al. A Compact Ka-Band Low-Sidelobe Monopulse Antenna Array Based on Mixed Gap Waveguide and Hollow Waveguide Multilayer Feeding Network, *IEEE Transactions on Antennas and Propagation*, vol. 71, no. 11, pp. 8714–8725, Nov. (2023).
27. Mohammadpour, M., Mohajeri, F. & Razavi, S. A. Aug., H-plane gap-RGW horn antenna with very low side lobe level. *Sci. Rep.*, **14**, 18289, (2024).
28. Huang, R., Wu, Y., Wu, L., Ran, J. & Wang, W. Dual Circularly Polarized Diplexer-Antenna Array with Low-Sidelobe Level Based on Gap Waveguide at Ka-Band, *IEEE Antennas and Wireless Propagation Letters*, vol. 23, no. 10, pp. 2959–2963, Oct. (2024).
29. Pla-Herliczka, D., Herranz-Herruzo, J. I., Ferrando-Rocher, M. & Valero-Nogueira, A. Taylor-Weighting Ridge Gap Waveguide Feed Network for Low-Profile Fully Metallic Array Antennas, *IEEE Antennas and Wireless Propagation Letters*, vol. 23, no. 9, pp. 2703–2707, Sept. (2024).
30. Zhang, L. et al. Feb., A Single-Layer 10–30 GHz Reflectarray Antenna for the Internet of Vehicles, *IEEE Transactions on Vehicular Technology*, vol. 71, no. 2, pp. 1480–1490, (2022).
31. Badisa, A. B. et al. Design and analysis of AMC reflector integrated flexible and compact vehicular antenna for Communication Application. *Radioelectron Commun. Syst.* **65**, 411–419 (2022).
32. Wang, P. et al. Wideband Transmit-Array Antenna Design with Dual-Layer Ultrathin Huygens' Meta-Surface for Vehicular Sensing and Communication. *IEEE Trans. Veh. Technol.* **72** (6), 7469–7479 (June 2023).
33. Raju, M. P. Design and Analysis of Printed Conformal Antenna System for Inter and Intra Vehicular (V2V) Communication Utilizations. *Progress Electromagnet. Res. C.* **142**, 143–150 (2024).
34. Lee, K. H., Yun, S. J., Lee, J. N. & Cho, Y. K. A Compact Slotted Waveguide Array Antenna with a Cubic Post Radiator for Aerial Vehicle Applications. *IEEE Access.* **12**, 69301–69309 (2024).
35. R. C. Hansen, *Phased Array Antennas*, 2nd ed. Hoboken, NY, USA: Wiley, (2009).

Author contributions

D. Z. contributed to the conceptualization and design of the study and was involved in the drafting and revision of the manuscript. A. S. S. contributed to the conceptualization and design of the study. A. U. Z. supervised the design and was involved in the drafting and revision of the manuscript.

Declarations

Competing interests

The authors declare no competing interests.

Additional information

Correspondence and requests for materials should be addressed to D.Z.

Reprints and permissions information is available at www.nature.com/reprints.

Publisher's note Springer Nature remains neutral with regard to jurisdictional claims in published maps and institutional affiliations.